NANO LETTERS

Letter

pubs.acs.org/NanoLett

Bismuth-Catalyzed and Doped Silicon Nanowires for One-Pump-Down Fabrication of Radial Junction Solar Cells

Linwei Yu,[†,*] Franck Fortuna,[‡] Benedict O'Donnell,[†,§] Taewoo Jeon,[†] Martin Foldyna,[†] Gennaro Picardi,[†] and Pere Roca i Cabarrocas[†]

[†]LPICM, Ecole Polytechnique, CNRS, 91128 Palaiseau, France

[‡]CSNSM, Université Paris-Sud, Bâtiment 108, 91405 Orsay Campus, France

[§]R&D Division, Total S.A., Gas & Power, Courbevoie, France

ABSTRACT: Silicon nanowires (SiNWs) are becoming a popular choice to develop a new generation of radial junction solar cells. We here explore a bismuth- (Bi-) catalyzed growth and doping of SiNWs, via vapor−liquid−solid (VLS) mode, to fabricate amorphous Si radial n−i−p junction solar cells in a one-pump-down and low-temperature process in a single chamber plasma deposition system. We provide the first evidence that catalyst doping in the SiNW cores, caused by incorporating Bi catalyst atoms as n-type dopant, can be utilized to fabricate radial junction solar cells, with a record open circuit voltage of V_{oc} = 0.76 V and an enhanced light trapping effect that boosts the short circuit current to J_{sc} = 11.23 mA/cm^2. More importantly, this bi-catalyzed SiNW growth and doping strategy exempts the use of extremely toxic phosphine gas, leading to significant procedure simplification and cost reduction for building radial junction thin film solar cells.

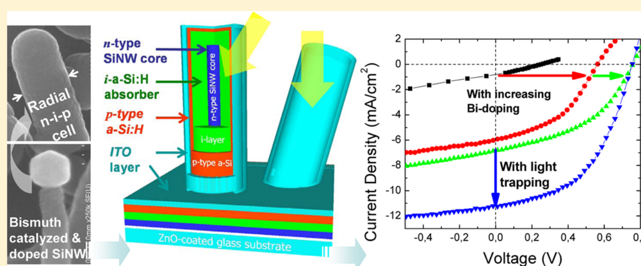

KEYWORDS: *Radial junction solar cell, silicon nanowire, vapor−liquid−solid growth, bismuth catalyzed growth, bismuth doping, PECVD thin film deposition*

Building radial junction thin film solar cells on top of silicon nanowires (SiNWs) allows to decouple light absorption path from photocarrier collection distance, making it possible to reduce the absorber thickness to improve carrier collection, while still achieving enhanced light trapping among SiNWs.[1−5] Amorphous and microcrystalline Si thin film technologies are industrially proven, environmentally friendly and capable of delivering Terawatt scale solar energy without fundamental limitation in material supply.[6,7] Marrying the advanced radial junction design to this mature Si thin film technology has thus the potential to build up a high performance and cost-effective thin film photovoltaics (PV). Particularly, by adopting a thinner absorber layer in a radial junction configuration, a stronger built-in field can help to minimize the Staebler-Wronski degradation in hydrogenated amorphous Si (a-Si:H) cells. To this end, a first and primary concern is to establish a SiNWs growth strategy compatible with the industrial-mainstream plasma deposition process, ideally achieving it on top of cost-effective substrates and at low temperature. The vapor−liquid−solid (VLS) mechanism represents a high-throughput and cost-effective way to produce well-defined SiNWs on top of various low-cost substrates.[8−11] However, since the VLS growth has to be catalyzed by metal nanoparticles, the remnant of metal catalysts on/in SiNWs imposes usually a threat to building effective photovoltaics, where clean surface/interfaces and minimum recombination centers are of utmost importance. Widely used gold (Au) is known to introduce midgap defects in c-Si,[12] acting as recombination centers for photocarriers. As a consequence, prototype SiNW solar cells built on top of untreated Au-catalyzed SiNWs show usually a low open circuit voltage (V_{oc}) < 0.3 V and poor fill factors (FF) < 30%.[3,13−15] High temperature (>900 °C) oxidation and chemical wet etching are therefore required to alleviate/suppress this impact.[2] Fortunately, VLS growth allows for a vast choice of alternative catalysts.[16] We have been working on a group of low-melting-point metals such as indium (In), tin (Sn), and gallium to achieve a low-temperature SiNW growth (down to 240 °C) in a plasma enhanced chemical vapor deposition (PECVD) environment.[17−23] An additional advantage lies in the fact that these catalysts can be eventually removed from the SiNWs by a simple H_2 plasma etching, while the incorporation of catalyst atoms into c-Si introduces only shallow or neutral levels in the Si bandgap. These features make them attractive to fabricate SiNW-based radial junction solar cells in an all-*in situ* or one-pump-down CVD process.

In this work, we explore the use of bismuth (Bi) as catalyst to mediate the VLS growth of SiNWs, and provide the first evidence that Bi-catalyst incorporation in the c-SiNW cores can be utilized to achieve simultaneously effective n-type doping for building radial n−i−p junction solar cells. Bi has been known to introduce a shallow donor level in c-Si, lying 69 meV below the

Received: May 7, 2012
Revised: July 13, 2012
Published: July 23, 2012

Downloaded via NANJING UNIV on October 27, 2025 at 13:53:31 (UTC).
See https://pubs.acs.org/sharingguidelines for options on how to legitimately share published articles.

ACS Publications © 2012 American Chemical Society

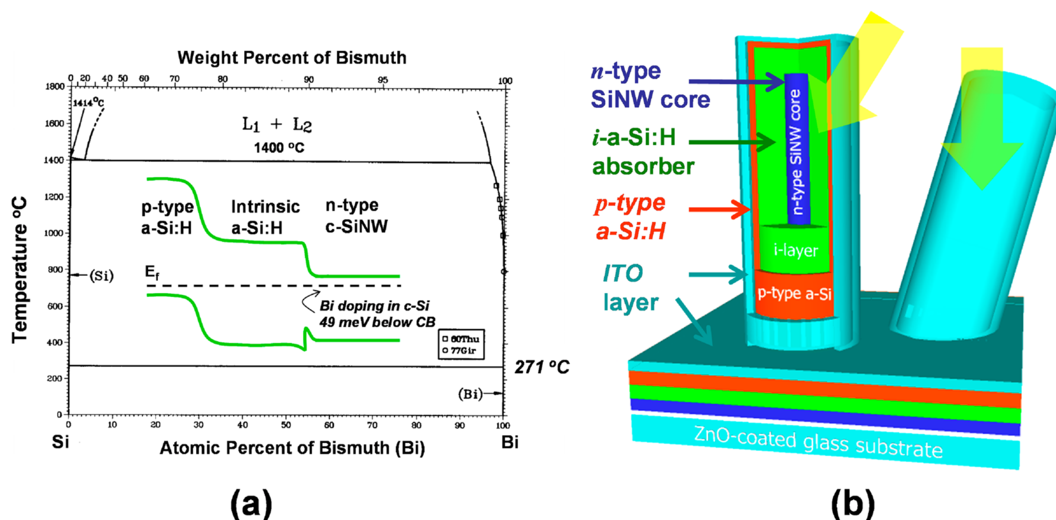

Figure 1. (a) Binary phase diagram of Si–Bi alloy, according to ref 24., while the center inset illustrates the doping level position of Bi dopant in the bandgap of c-Si, which is 0.069 eV below the conduction band bottom. (b) Schematic illustration of the radial junction thin film solar cell multilayer structure built over bi-catalyzed SiNWs on top of ZnO-coated glass substrate.

conduction band edge, indicated in the inset of Figure 1a,[12,16] with an eutectic point with Si at 271.4 °C and relatively low Si solubility (see the phase diagram in Figure 1a[24]). But Bi has been scarcely explored to catalyze the growth of SiNWs, owing partially to the Nebol'sin criterion,[25] saying that low-surface-tension (LST) catalysts (Bi features a low surface tension of 0.37 N/m)[26] pose a fundamental difficulty for a unidirectional growth of SiNWs. Somewhat in contrast to this belief, our recent research on similar LST metals such as Sn or In for catalyzing VLS growth of SiNWs, has revealed a new growth stability mechanism for the LST catalysts.[23] We demonstrate here a Bi-catalyzed growth of SiNWs via VLS mechanism in a conventional PECVD system, where the incorporation of Bi catalyst atoms causes effective n-type doping in the as-grown SiNWs. This has enabled us to complete a n-type SiNW-core/intrinsic a-Si:H/p-type a-Si:H radial junction cell in a one-pump-down plasma deposition process, without the use of toxic phosphine gas. Using this approach we have been able to achieve simultaneously a record open circuit voltage of V_{oc} = 0.76 V (among all the reported radial n–i–p junction thin film solar cells) and an strongly enhanced light trapping to boost the short-circuit current. This Bi-catalyzed growth and doping strategy exempts the use of extremely hazardous phosphine gas and avoids the cross-contamination from using two dopants, leading to significant procedure simplification and cost reduction for building radial junction thin film solar cells.

Moreover, as illustrated in Figure 1b, when shedding incident light through the top emitter layer, a high concentration of photocarriers will be generated close to the outer emitter/absorber interface. Considering that the hole mobility is much lower than that of electrons in the a-Si:H absorber, a p-type emitter is always preferable in order to facilitate carrier separation and minimize recombination in the intrinsic layer.[6,27] In view of this, a bi-catalyzed n-type SiNW core represents a favorable choice for building n-core/i-absorber/p-emitter radial junction thin film solar cells.

SiNWs were grown on top of Al-doped ZnO (~2 μm)/glass substrates, coated with a thin layer of Bi of 0.3 - 18.5 nm (nominal thickness determined by a quartz microbalance). The substrates were loaded into a capacitively coupled PECVD chamber and exposed to a H_2 plasma at 300 °C for 90 s, with H_2 flow rate, chamber pressure and RF power density of 100 sccm, 380 mTorr, and 53 mW/cm^2, respectively. During the H_2 plasma treatment, nanoscale Bi droplets were formed as a result of surface diffusion and coalescence of Bi atoms on the ZnO surface (as illustrated schematically in Figure 2a). Without

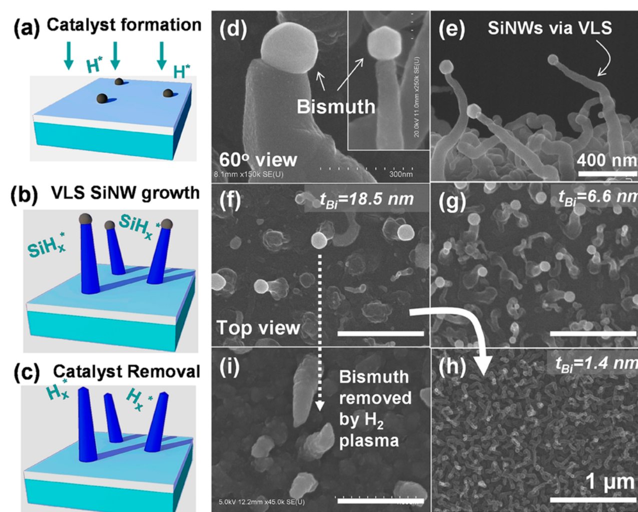

Figure 2. (a–c) Respectively, *in situ* Bi catalyst formation, SiNW growth, and catalyst etching processes in a PECVD system; (d, e) side-view SEM images of the bi-catalyzed SiNW growth via a typical VLS mode. Top-view SEM images of SiNWs grown with a Bi layer thickness of t_{Bi} = 18.6, 6.6, and 1.4 nm are shown in parts f–h, respectively. (i) SEM image of the SiNWs after being treated by *in situ* H_2 etching to remove the bi-catalyst drops on top.

breaking the vacuum, the substrate temperature was raised to 450 °C and a mixture of 100 sccm H_2 and 10 sccm SiH_4 gas was introduced to trigger the growth of SiNWs, as depicted by Figure 2b, with typical chamber pressure, RF power density and deposition time of 600 mTorr, 22 mW/cm^2 and 20 min, respectively. As seen in the scanning electron microscopy (SEM) images in Figure 2d,e, bright Bi droplets can be found at the tip of SiNWs, indicating a bimediated VLS growth process. In this study, the Bi layer thickness has been used as a major

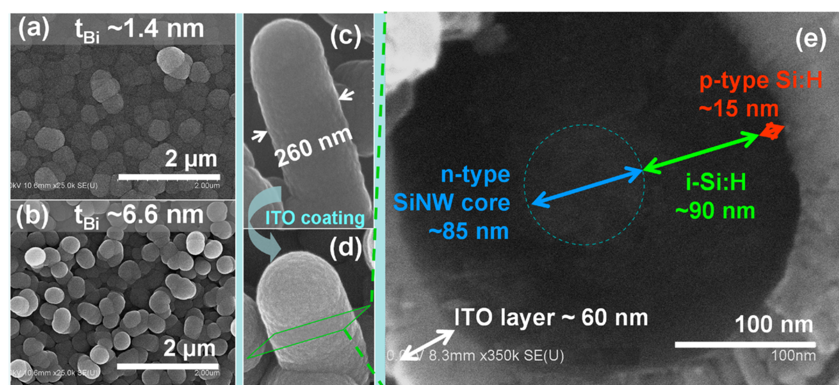

Figure 3. (a and b) Radial junction structures fabricated on top of the SiNWs grown from an initial Bi layer thickness of t_{Bi} = 1.4 nm and t_{Bi} = 6.6 nm, respectively. A close side-view SEM image of a single SiNW radial junction (grown with t_{Bi} = 6.6 nm) is presented in part c, with the final SiNW cell with top ITO contact shown in part d. The coaxial multilayer structure in the radial junction can be seen in a cross-section SEM image of a truncated SiNW-cell shown in part e.

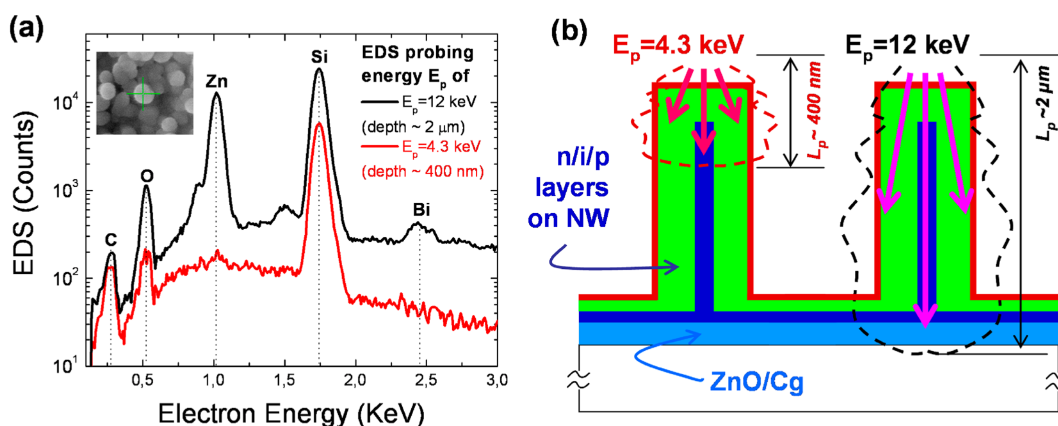

Figure 4. (a) EDS spectra measured on Bi-catalyzed SiNW radial junction at two probing energies (E_p = 4.3 keV and E_p = 12 keV), positioned at the tips of radial junction unit (without ITO coating) as indicated by the green cross in the top-left inset SEM image. (b) Schematic illustration of the different effective probing regions and depths (L_p) of the EDS analysis under different probing energies.

parameter to control the size and distribution of the catalyst droplets (and thus the SiNWs grown from them). Top view SEM images of the SiNWs grown from initial Bi layer thickness of t_{Bi} = 18.5, 6.6, and 1.4 nm are presented respectively in Figure 2, parts f−h. With a decreasing initial Bi thickness, the produced SiNWs become smaller but with a higher density.

As seen in Figure 2h, in case of a Bi layer thickness of t_{Bi} = 1.4 nm, there are basically no Bi catalyst droplets that could be found on top of the SiNWs after 20 min of plasma deposition. This could result from i) the evaporation of Bi during growth (at 450 °C); ii) the incorporation of Bi atoms into the SiNWs, or iii) the formation of a volatile compound of Bi in H_2 plasma environment. Considering the extremely low solubility of Bi in c-Si ($<10^{-5}$ at 800 °C),[24] the incorporation of Bi into SiNWs cannot be a major reason for the disappearance of Bi catalyst drops. Actually, Bi is known to have a relatively higher vapor pressure than Sn and In, and could form volatile trihydride compound in a H_2 plasma environment.[28] To verify this hypothesis, we chose a sample with an initial Bi layer thickness of 18.5 nm and grew SiNWs with clearly large Bi catalyst drops resting on top, as seen for example in Figure 2f. Then, a H_2 plasma treatment (immediately after the VLS growth) was applied for 30 min, as illustrated in Figure 2c. We found that even the large Bi catalyst drops of several hundreds of nanometers can be completely removed, as witnessed in Figure 2i. This proves that Bi catalyst drops can be completely removed by an *in situ* H_2 plasma treatment, indicating a critical ability to integrate the VLS-grown SiNWs into standard Si thin film solar cell fabrication process.

Choosing SiNW growth conditions with initial thickness of t_{Bi} = 6.6 nm and t_{Bi} = 1.4 nm, we proceeded to the fabrication of radial junction n−i−p solar cells on top of the SiNWs, which involves the following: (i) first, the deposition of an intrinsic a-Si:H layer (~100 nm) at 180 °C, with 100 sccm SiH_4, 120 mTorr, and RF power density of 12 mW/cm^2; followed by (ii) the deposition of p-type a-Si:H emitter layer (~10 nm) by adding 1 sccm Trimethylboron (TMB) dopant gas. In parts a and b of Figure 3, we show the radial junction structures fabricated on top of the SiNWs, grown from an initial Bi layer thickness of t_{Bi} = 1.4 nm and t_{Bi} = 6.6 nm, respectively. A close side-view SEM image of a single SiNW radial junction with a total diameter of ~260 nm is presented in Figure 3c. To verify the catalyst removal and evaluate the remnant Bi catalyst presence among the final radial junction structures, energy dispersion spectroscopy (EDS) measurement were performed to analyze the chemical composition in the long SiNW sample (with t_{Bi} = 6.6 nm). The probing points were positioned at the tips of the radial junction cells in the region without ITO coating (as indicated, for example, by the green cross in the top-left inset in Figure 4a). Two different probing electron energies of E_p = 4.3 keV and E_p = 12 keV were used, corresponding to a penetration depth of ~400 nm and ~2 μm

dx.doi.org/10.1021/nl3017187 | *Nano Lett.* 2012, 12, 4153−4158

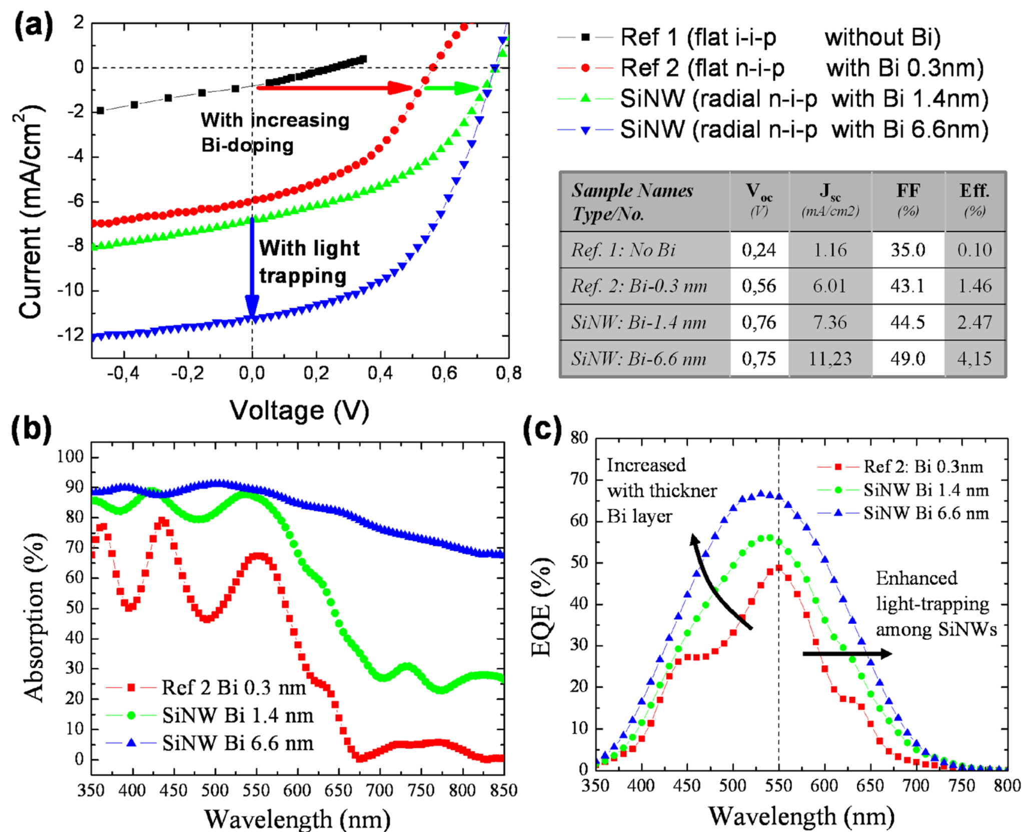

Sample Names Type/No.	V_{oc} (V)	J_{sc} (mA/cm2)	FF (%)	Eff. (%)
Ref. 1: No Bi	0,24	1.16	35.0	0.10
Ref. 2: Bi-0.3 nm	0,56	6.01	43.1	1.46
SiNW: Bi-1.4 nm	0,76	7.36	44.5	2.47
SiNW: Bi-6.6 nm	0,75	11,23	49.0	4,15

Figure 5. (a) $J-V$ characteristics of the Bi-catalyzed SiNW radial junction solar cells and the reference flat junction devices (with or without Bi-doping). The corresponding solar cell parameters are summarized in the bottom-right insight. (b and c) Absorption and external quantum efficiency characterizations of the corresponding samples.

respectively. The effective EDS probing volume (into the radial junction structure) under different probing energies are illustrated in Figure 4b. With a penetration depth of $L_p \sim$ 400 nm at E_p = 4.3 keV, the EDS signal (seen as the red curve in Figure 4a) reveals basically the composition of the upper segment of the radial n−i−p junction (since $L_p < L_{SiNW} \sim 1.5$ μm), which includes the a-Si:H coating layers of p-type emitter, intrinsic absorber and the tip/core of the SiNW. Among several sampling tests, no Bi catalyst remnant signal could be detected in the radial junction (putting an up-bound concentration <0.1% by the detector resolution). By increasing the probing energy to E_p= 12 keV, the probing zone extends to $L_p \sim 2$ μm > L_{SiNW} and thus covers effectively the whole radial junction, as depicted in Figure 4b, as well as the surface thin film and the under beneath ZnO/glass substrate. In this case, the EDS curve of E_p = 12 keV in Figure 4a reveals a trace of Bi catalyst, accompanied with a strong Zn signal arising from the ZnO layer. This suggests that a small portion of Bi catalyst drops, that were not activated to mediate SiNW growth, might be buried by a codeposited a-Si:H layer at the bottom surface during the plasma enhanced deposition. These EDS measurements confirm again that the Bi catalyst drops can be indeed completely removed from the SiNWs structure, leaving a clean 3D framework to build up a radial junction thin film solar cell.

Finally, transparent top electrodes (of 0.126 cm^2) were made by sputtering 80 nm ITO layer through a shadow mask, to allow the incident light shedding from top. The SEM image in Figure 3d shows an ITO-coated radial p-i-n junction, while Figure 3e provides a detailed cross-section SEM image of the coaxial multilayers in a truncated SiNW-cell. Current density (J) − voltage (V) curves of the bi-catalyzed SiNW radial junction solar cells were then measured under standard AM1.5G illumination (Newport's Oriel Sol3A Solar Simulator) at 25 °C and shown in Figure 5a. Two reference samples were also fabricated following the same deposition procedure, except that in the Ref_1 sample there was no Bi catalyst layer on the ZnO/Cg substrate (hereby, named as flat i−i−p), while in the Ref_2 sample the Bi layer is only ~0.3 nm, which leads to no SiNWs growth but introduces Bi diffusion into the a-Si:H layer (named as flat n−i−p). The characteristics of the solar cells are summarized in the right-inset table in Figure 5a. We see that the doping effect of Bi on both the SiNWs and the flat a-Si:H samples is significant: comparing reference samples Ref_1 and Ref_2 in Figure 5a, even a δ-doping-like Bi layer of 0.3 nm can lead to a 2-fold (or 5-fold) increase in the V_{oc} (or J_{sc}), providing a first proof for the n-type doping effect of Bi. In the sample with a Bi layer of 1.4 nm, Bi-catalyzed SiNWs start to grow into ~500 nm long and 35−50 nm wide in diameter, as seen for example in the SEM image in Figure 2h. Bi-doping of the c-Si cores leads to a further increase of open circuit voltage up to V_{oc} =0.76 V, while increasing the short circuit current to J_{sc} = 7.36 mA/cm^2. The increased V_{oc} could arise from a higher concentration of Bi dopants in the SiNWs, or/and a more effective ionization/activation rate of the Bi dopants in the crystalline SiNW cores, compared to the doping effect of Bi in a-Si:H matrix, where a higher defect density and a wider bandgap (~1.7 eV for a-Si:H) will limit the ionization rate of the dissolved Bi atoms. Further on, in the radial junction solar cells constructed on top of longer (~1.5 μm) and thicker (with diameter of 60−100 nm) SiNWs, grown from a 6.6 nm Bi layer,

dx.doi.org/10.1021/nl3017187 | Nano Lett. 2012, 12, 4153−4158

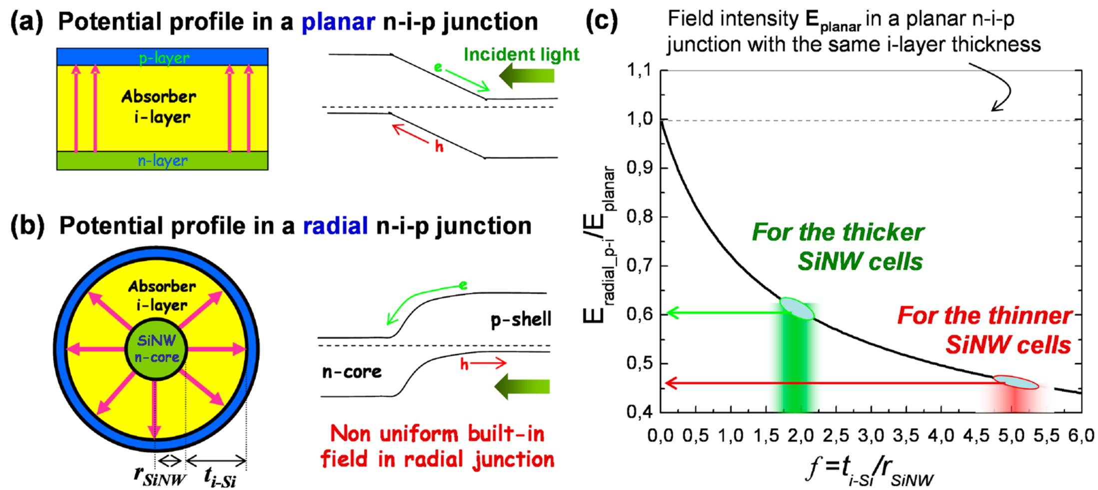

Figure 6. (a and b) Different potential profile and built-in field distribution in a planar or a radial n−i−p junction. (c) Plots of the ratio between the built-in field intensity at the outer p−i interface in a radial n−i−p junction (E_{radial_p-i}) and that in a planar junction (E_{planar_p-i}), as a function of a geometrical factor $f \equiv t_{i-Si}/r_{SiNW}$. The corresponding situations for the thinner ($r_{SiNW} \sim 40$ nm) or thicker ($r_{SiNW} \sim 80$ nm) SiNWs in this study are marked respectively by the red and green lines/circles.

a significant gain in the short circuit current has been obtained, bringing J_{sc} to 11.23 mA/cm^2, while the open circuit voltage V_{oc} remains basically the same. This behavior highlights the benefits of a strong light trapping effect achieved among a longer SiNWs *matrix*. This is also consistent with the trend observed in their absorption spectra (A) shown in Figure 5b, which were obtained by subtracting corresponding transmission (T) and reflection (R) spectra ($A = 1 - T - R$), measured at normal incidence with a UV/vis/NIR Lambda-950 spectrophotometer with an integrating sphere (PerkinElmer-150 mm InGaAs). In general, the SiNWs radial junction cells demonstrate a stronger absorption over a broad spectrum of incident light. We note that the open circuit voltage of 0.76 V has been achieved with only a single dopant gas (TMB gas for p-emitter), and it has been close to the record V_{oc} = 0.81 V among all the radial junction solar cells (reported in our previous studies[29−31] in a radial p−i−n configuration with both phosphine and TMB dopants for *p*- and *n*-doping layers, respectively.) This emphasizes again the effective n-type doping of Bi catalyst, during the VLS growth of c-SiNW, and opens a new dimension for implementing the VLS-grown SiNWs for photovoltaics and other electronic applications.

The ideality factors n of the radial junction diode, extracted from the dark J−V curves, $J_{dark} \sim e^{V/(n \cdot kT)}$, under forward bias condition in the range of V = 0.3−0.5 V, are found to be respectively 1.95, 2.01, and 2.14 for the flat Ref_2 sample (with Bi:0.3 nm), the SiNW-Bi:1.4 nm and the SiNW-Bi:6.6 nm samples. This indicates that the carrier transport in the radial junction diodes is dominated by carrier recombination, which is typical for thin film solar cells with a-Si:H as absorber, where the carrier diffusion length is short and carrier recombination accounts for the major transport mechanism across the n-i-p junction. According to the external quantum efficiency (EQE) spectra, measured with a calibrated silicon detector (Newport 70356 module) and shown in Figure 5c, the spectral response is that of a typical a-Si:H cell, indicating that only the intrinsic a-Si:H layer is photon-active, while the Bi-doped crystalline SiNW core (under current growth condition) is inactive or has negligible contribution to photocurrent generation. Comparing the EQE spectra shown in Figure 5c, the red-shifting of the long-wavelength edge reflects the contribution of an enhanced light trapping among a 3D radial junction architecture. However, the EQE response registers also an obvious enhancement in the short-wavelength region (<550 nm), which cannot be simply assigned to the light trapping effects since high energy photons are usually absorbed during their first pass through the n−i−p junction. Moreover, in the range of high photon energy (350 to 550 nm), the absorption spectra of the longer and shorter SiNW cells differ only by <5% on average, as seen in Figure 5b, which by itself could not explain a much larger response difference of ∼20% to 30% in the same wavelength range, as witnessed in Figure 5c. Given a similar absorber and p-type emitter layer thickness, the underlying reason for the different internal quantum efficiency (defined as IQE = EQE/absorption) must be related to the carrier collection and separation in the radial n−i−p junction structure.

In a typical a-Si:H thin film solar cell, photocarrier separation and collection rely heavily on the sweeping built-in field in the intrinsic layer. Comparing a radial junction cell (Figure 6b) to a planar counterpart (Figure 6a), an obvious difference comes from the fact that the incident light (indicated by the green arrows) can only be shed from the outer p-type emitter. Thus, a high concentration of photocarriers will be first generated in the region close to the outer p−i interface, which is particularly true for the absorption of high energy photons. A strong built-in field in the i-layer, particularly at the *p-i* interface, is critical to minimize carrier recombination and facilitate carrier separation. In contrast to a basically uniform built-in field in a planar n−i−p junction, with $E_{planar}(t_{i-Si}) \equiv V_{oc}/t_{i-Si}$, as illustrated in the inset of Figure 6a, the built-in field in a radial junction is established by a pair of asymmetrical electrodes with different facing areas, as depicted for instance in Figure 6b, and thus becomes nonuniform over the *i*-layer. Specifically, when coating on top of a SiNW with radius of r_{SiNW}, the built-in field in a radial *i*-layer is described as a function of the distance t, measured from the *n-i* interface, as

$$E_{radial}(t) = \frac{V_{oc}}{(r+t)\ln(1+t/r)} = E_{planar}(t)\frac{1}{(1+r/t)\ln(1+t/r)} \quad (1)$$

As a consequence, $E_{radial}(t)$ in the radial junction will decreases gradually from the maximum field intensity of $E^{max}_{radial_n-i} = E_{planar}$ at the inner n−i interface, to the minimum intensity of E_{radial_p-i} at the outer p−i interface. In particular, at the outer p−i interface, the ratio of the radial junction building field over that in a planar counterpart, with the same intrinsic layer thickness, can be written as

$$E_{radial\,p-i}/E_{planar} = \frac{1}{(1+1/f)\ln(1+f)} \quad (2)$$

where $f = t_{i-Si}/r_{SiNW}$.

Figure 6c gives a plot of this ratio, as a function of the geometrical factor f (defined as the ratio of the coating layer thickness over the SiNW radius), showing that E_{radial_p-i} decreases as the SiNW core becomes thinner (larger f). Assuming a similar i-layer of $t_{i-Si} \sim 90$ nm has been deposited on top of the SiNWs, a thicker SiNW core has the advantage to sustain a stronger built-in field at the outer p−i interface. Corresponding situations for the thinner (30−50 nm) and thicker (60−100) SiNW structures in this study are also marked in Figure 6c, indicating that the p−i interface built-in field in a thicker SiNW cell (indicated by the green lines) could be ~33% stronger than that in the thinner SiNW cell (by the red lines). As a stronger sweeping field at the p−i interface will help to separate and collect the high concentration of photocarriers generated close to the p−i interface (particularly for those by the high energy photons), this could explain, from a geometrical perspective, the enhanced EQE response of the thicker SiNW cells in the high energy photon regime (<550 nm) over the thinner ones.

In summary, we have demonstrated a bi-catalyzed growth and doping of SiNWs via VLS mode, and apply them to construct radial junction thin film solar cells in a one-pump-down and low temperature deposition process in a conventional PECVD system. The effective bi-doping in the c-SiNW cores helps to achieve both a high open-circuit voltage and enhanced light trapping effects, while exempting the use of toxic phosphine gas and simplifying the fabrication for a radial junction thin film solar cell. We have also demonstrated a catalyst self-cleaning of the bi-catalyzed VLS growth, and investigated systematically their absorption, external quantum efficiency and carrier collection in the radial junction thin film solar cell. These results lay a solid basis for establishing an *in situ* SiNW growth and catalyst-doping control aiming for a new generation of high efficiency Si thin film photovoltaics.

AUTHOR INFORMATION

Corresponding Author

*E-mail: Linwei.yu@polytechnique.edu.

Notes

The authors declare the following competing financial interest(s): A patent has been filed based on this work.

ACKNOWLEDGMENTS

This work has been performed in the TOTAL-LPICM joint PV Research Team, LPICM, Ecole Polytechnique/CNRS. The research at CSNSM has been supported by Triangle de la physique, Contract No. 2009-082T

REFERENCES

(1) Peng, K.-Q.; Lee, S.-T. *Adv. Mater.* **2011**, *23* (2), 198−215.
(2) Kendrick, C. E.; Yoon, H. P.; Yuwen, Y. A.; Barber, G. D.; Shen, H.; Mallouk, T. E.; Dickey, E. C.; Mayer, T. S.; Redwing, J. M. *Appl. Phys. Lett.* **2010**, *97* (14), 143108−3.
(3) Gunawan, O.; Guha, S. *Sol. Energy Mater. Sol. Cells* **2009**, *93* (8), 1388−1393.
(4) Lu, Y.; Lal, A. *Nano Lett.* **2010**, *10* (11), 4651−4656.
(5) Garnett, E.; Yang, P. *Nano Lett.* **2010**, *10* (3), 1082−1087.
(6) Shah, A. V.; Schade, H.; Vanecek, M.; Meier, J.; Vallat-Sauvain, E.; Wyrsch, N.; Kroll, U.; Droz, C.; Bailat, J. *Prog. Photovoltaics: Res. Appl.* **2004**, *12* (2−3), 113−142.
(7) Feltrin, A.; Freundlich, A. In *Material Challenges for Terawatt Level Deployment of Photovoltaics*; Conference Record of the 2006 IEEE 4th World Conference on Photovoltaic Energy Conversion, May 2006; Waikoloa, HI; **2006**; pp 2469−2472, DOI: 10.1109/WCPEC.2006.279727.
(8) Givargizov, E. I. *J. Cryst. Growth* **1975**, *31*, 20−30.
(9) Lieber, C. M. *Mater. Res. Bull.* **2003**, *28*, 486−491.
(10) Wei, L.; Charles, M. L. *J. Phys. D: Appl. Phys.* **2006**, *39* (21), R387.
(11) Rurali, R. *Rev. Mod. Phys.* **2010**, *82* (1), 427.
(12) Sze., S. M. *Physics of Semiconductor Devices*, 2nd ed.; Wiley: New York, 1981; Vol. *1*.
(13) Perraud, S.; Poncet, S.; Noël, S.; Levis, M.; Faucherand, P.; Rouvière, E.; Thony, P.; Jaussaud, C.; Delsol, R. *Sol. Energy Mater. Sol. Cells* **2009**, *93* (9), 1568−1571.
(14) Th, S.; Pietsch, M.; Andr, G.; Falk, F.; Ose, E.; Christiansen, S. *Nanotechnology* **2008**, *19* (29), 295203.
(15) Tsakalakos, L.; Balch, J.; Fronheiser, J.; Korevaar, B. A.; Sulima, O.; Rand, J. *Appl. Phys. Lett.* **2007**, *91* (23), 233117.
(16) Volker, S.; Joerg, V. W.; Stephan, S.; Ulrich, G. *Adv. Mater.* **2009**, *21* (25−26), 2681−2702.
(17) Alet, P.-J.; Yu, L.; Patriarche, G.; Palacin, S.; Roca i Cabarrocas, P. *J. Mater. Chem.* **2008**, *18* (43), 5187−5189.
(18) Yu, L.; Alet, P.-J.; Picardi, G.; Maurin, I.; Roca i Cabarrocas, P. *Nanotechnology* **2008**, *19* (48), 485605.
(19) Yu, L.; O'Donnell, B.; Alet, P.-J.; Conesa-Boj, S.; Peiro, F.; Arbiol, J.; Roca i Cabarrocas, P. *Nanotechnology* **2009**, *20* (22), 225604.
(20) Zardo, I.; Yu, L.; Conesa-Boj, S.; Estrade, S.; Alet, P. J.; Rossler, J.; Frimmer, M.; Roca i Cabarrocas, P.; Peiro, F.; Arbiol, J.; Morante, J. R.; Fontcuberta i Morral, A. *Nanotechnology* **2009**, *20* (15), 155602.
(21) Yu, L.; O'Donnell, B.; Maurice, J.-L.; Roca i Cabarrocas, P. *Appl. Phys. Lett.* **2010**, *97* (2), 023107−3.
(22) Zardo, I.; Conesa-Boj, S.; Estradé, S.; Yu, L.; Peiro, F.; Roca i Cabarrocas, P.; R. Morante, J.; Arbiol, J.; Fontcuberta i Morral, A. *Appl. Phys. A: Mater. Sci. Processing* **2010**, *100* (1), 287−296.
(23) Yu, L.; Fortuna, F.; O?Donnell, B.; Patriache, G.; Roca i Cabarrocas, P. *Appl. Phys. Lett.* **2011**, *98* (12), 123113.
(24) Olesinski, R.; Abbaschian, G. *J. Phase Equilib.* **1985**, No. 4, 359−361.
(25) Nebol'sin, V. A.; Shchetinin, A. A. *Inorg. Mater.* **2003**, *39* (9), 899−903.
(26) Keene, B. J. *Int. Mater. Rev.* **1993**, *38* (4), 157.
(27) Green, M. *J. Mater. Sci.: Mater. Electron.* **2007**, *18* (0), 15−19.
(28) Baran, J., E., *Vibrational properties of bismutine, BiH[3]*. Verlag der Zeitschrift für Naturforschung: Tübingen, Germany, 2003; Vol. *58*, pp 126−128.
(29) O'Donnell, B.; Yu, L.; Foldyna, M.; Roca i Cabarrocas, P. *J. Non-Cryst. Solids* **2011**, DOI: 10.1016/j.jnoncrysol.2011.11.026, (0).
(30) Cho, J.; O'Donnell, B.; Yu, L.; Kim, K.-H.; Ngo, I.; Roca i Cabarrocas, P. *Prog. Photovoltaics: Res. Appl.* **2011**, DOI: 10.1002/pip.1245.
(31) Yu, L.; O'Donnell, B.; Foldyna, M.; Roca i Cabarrocas, P. *Nanotechnology* **2012**, *23*, 194011.